**Generation of a 3D proximal femur shape from a single projection 2D radiographic image.**

Langton C M[1,2], Pisharody S[3], Mathers C[1], Keyak J H[4]

[1]Centre for Metabolic Bone Disease, Hull Royal Infirmary, Hull, UK

[2]Postgraduate Medical Institute, University of Hull, Hull, UK

[3]Department of Computer Science, University of Hull, Hull, UK

[4]Department of Orthopaedic Surgery, University of California, Irvine, USA

Corresponding Author:

Professor C M Langton, Medical Physics, Queensland University of Technology, Brisbane, QLD 4001, Australia

Tel: +61 7 31382002

Email: christian.langton@qut.edu.au

**Mini Abstract**

Generalized Procrustes Analysis and Thin Plate Splines were employed to create an average 3D shape template of the proximal femur that was warped to the size and shape of an individual 2D radiographic image. Mean absolute depth errors are comparable with previous approaches utilising multiple 2D input projections.

**Abstract**

Introduction: Several approaches have been adopted to derive volumetric density (g $cm^{-3}$) from a conventional 2D representation of areal bone mineral density (BMD, g $cm^{-2}$). Such approaches have generally aimed at deriving an average depth across the areal projection rather than creating a formal 3D shape of the bone.

Methods: Generalized Procrustes Analysis and Thin Plate Splines were employed to create an average 3D shape template of the proximal femur that was subsequently warped to suit the size and shape of a single 2D radiographic image of an individual subject. CT scans of excised human femora, 18 and 24 scanned at pixel resolutions of 1.08 mm and 0.674 mm respectively, were equally split into training (created 3D shape template) and test cohorts.

Results: The mean absolute depth errors of 3.4 mm and 1.73 mm respectively for the two CT pixel sizes are comparable with previous approaches based upon multiple 2D input projections.

Conclusions: This technique has the potential to derive volumetric density from BMD and to facilitate 3D finite element analysis for prediction of the mechanical integrity of the proximal femur. It may further be applied to other anatomical bone sites such as the distal radius and lumbar spine.

**Keywords:** 3D shape, geometric morphometrics, proximal femur, volumetric density

## Introduction

Dual energy X-ray absorptiometry (DXA) is routinely performed at the osteoporotic fracture sites of wrist, hip and spine, and provides an areal measurement describing the bone mass within a projected area, with units of g $cm^{-2}$. Quantitative computed tomography (QCT) utilises a calibration phantom to convert Hounsfield number into a measure of volumetric bone density (g $cm^{-3}$) of the hip and spine. The subject radiation dose associated with QCT is approximately 10 times higher than for DXA, making use of DXA over QCT desirable [**1**].

Several approaches have been previously adopted to derive volumetric density (g $cm^{-3}$) from a conventional 2D DXA representation of areal bone mineral density (g $cm^{-2}$). Such approaches have generally aimed at deriving an average depth across the areal projection rather than creating a formal 3D shape of the bone. More consideration has been given to the lumbar vertebrae than the proximal femur. Few studies have quantified the accuracy of their approach. The lumbar vertebra has been considered to be of cuboid nature, where the depth is calculated simply as the square root of the cross-sectional area [**2-4**] or the mean vertebral width in the orthogonal direction [**5**]. Both scientific [**6**] and clinical [**7**] evaluation of the vertebra considered to be an elliptical cylinder have been performed, although both studies did not report a significant benefit in their volumetric approach. For assessment of the distal radius and ulna, an assumption of cylindrical geometry has been assumed [**8**]. For the proximal femur, the square root of projected area has also been clinically applied to the femoral neck [**9**, **10**]".

## The creation of a 3D Bone Shape from 2D images

Caponetti and Fanelli [**11**] developed a 3D reconstruction algorithm from two mutually orthogonal X-ray views of the femur, which was later improved upon by Nikkhade-Dehkordi et al. [**12**]. In both these cases, the femur was considered in sub-parts, each having a smooth, round surface. The 3D shape was estimated by median filtering and contour finding on different parts of the X-ray images and generating each sub-part using Hermite surface patches. Hermite surfaces are cubic parametric surface patches defined by four corner

points and the tangent vectors to the surface at the corner points [**13**]. The reconstructed femurs were compared to CT-scan models and 80% of the femur shafts were found to have less than 2mm error and 93% less than 4mm. Laporte et al. [**14**] introduced the concept of non-stereo corresponding contours (NSCC) based on contour identification from biplanar radiographs for 3D reconstruction of the distal femur. These were used by Kolta et al. [**15**] for reconstruction of the proximal femur from orthogonal biplanar DXA scans. The reconstructed models showed good accuracy as compared with high-resolution personalized CT-scan models for 25 cadaveric femurs with a reported mean absolute error of 0.8mm (95% of errors were less than 2.1mm with maximum errors of up to 7.8mm obtained on the greater and lesser trochanters).

The primary limitation of all of these techniques to create a 3D shape is that they inherently require a minimum of two 2D images to be available. With conventional DXA, only a single 2D image is obtained. The aim of this paper is to describe the application of geometric morphometric techniques to generate a 3D bone shape derived from a single projection 2D radiographic image.

A shape may be described by a set of landmark points that correspond to some identifiable features of the object. These landmark points are homogenous between and within populations for that object. Geometric Morphometric studies focus on the properties of landmarks for quantifying and analysing shape, combining the use of multivariate statistics with visualization techniques **[16].**

Zheng et al. **[17]** described a technique of 2D/3D reconstruction using a combination of statistical extrapolation and regularized shape deformation with an iterative non-rigid 2D point-matching algorithm applied to fluoroscopic images. The point-matching algorithm involved symmetric nearest-neighbour mapping and 2D thin plate splines-based deformation to find best-matched pairs between the images and the model. 11 cadaveric femurs were

used in the study and average reconstruction errors of 1.2mm and 1mm were obtained using 2- and 3-input fluoroscopic images respectively.

The methodology behind the approach in this paper has two phases, viz., creation of a generic 3D shape template from a 'training' cohort, and then adaptation of this template to suit the size and shape of a single 2D radiographic projection of an individual proximal femur within a 'test' cohort.

## Methods

### Proximal Femur CT scan data

Three sets of excised femora, each scanned by computed tomography (CT) on different machines (because of a change in location and equipment upgrade), were used to create the 3D Shape Template. They consisted of a) 18 femora from 8 males and 10 females; age, 52–92 years), b) 12 femora from 8 males and 4 females; age, 53–88 years, and c) 12 femora from 12 female donors; age, 45–94 years) **[18]**. Preparation of femora for CT scanning was identical, regardless of data set. Each femur was immersed in water and placed atop a calibration phantom for CT scanning. Each set of femora was scanned on a different CT scanner and used slightly different scanning parameters. Femora set (a) were scanned on a GE 9800 Research Scanner (GE Healthcare Technologies, Waukesha, WI) with a $K_2HPO_4$ (KHP) calibration phantom,**[19]** 320 × 320 matrix, and 1.08 mm pixels. Femora sets (b) and (c) were scanned on GE HiSpeed Advantage and GE CTI CT scanners, respectively (GE Healthcare Technologies, Waukesha, WI), with a calcium hydroxyapatite (CHA) phantom (Image Analysis, Inc., Columbia, KY), 512 × 512 matrix, and 0.674-mm pixels. All scans were obtained using 80 kVp, 280 mAs, with a 3 mm slice thickness and the standard reconstruction technique adopted.

### 2D Mappings

A ray casting technique was applied to the CT scan data for each proximal femur thereby creating 2D mappings of ’offset’, ’depth’, and BMD. The mappings express the data as 256 level grey-scale bitmaps, shown in Figure 1.

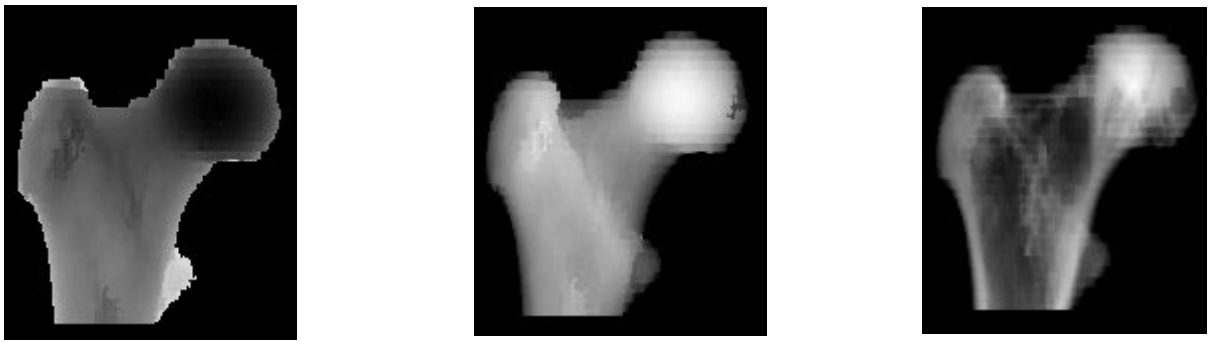

Figure 1: 2D ray casting mappings of offset (left), depth (centre), and BMD (right), expressed as 256 level greyscale images. Note that the femoral head and greater trochanter correspond to minimum offset but maximum depth and BMD.

For a column in a slice of the CT scan, ‘offset’ was defined as the number of voxels from the edge of the slice to the first bone voxel in that column (see Figure 2). ‘Depth’ was defined as the number of voxels from the first to the last bone voxel along the particular column. The depth map provided information about bone thickness at each pixel of a projected 2D radiograph image and the offset map provided the relative position of each part of the bone in the 3$^{rd}$ dimension, hence accounting for the protruding trochanteric section as well as the head anteversion. The BMD of each pixel within the BMD mapping (Figure 1c) was calculated with reference to the calibrated volumetric density data, following an integrated bone mineral content divided by area calculation as performed for DXA.

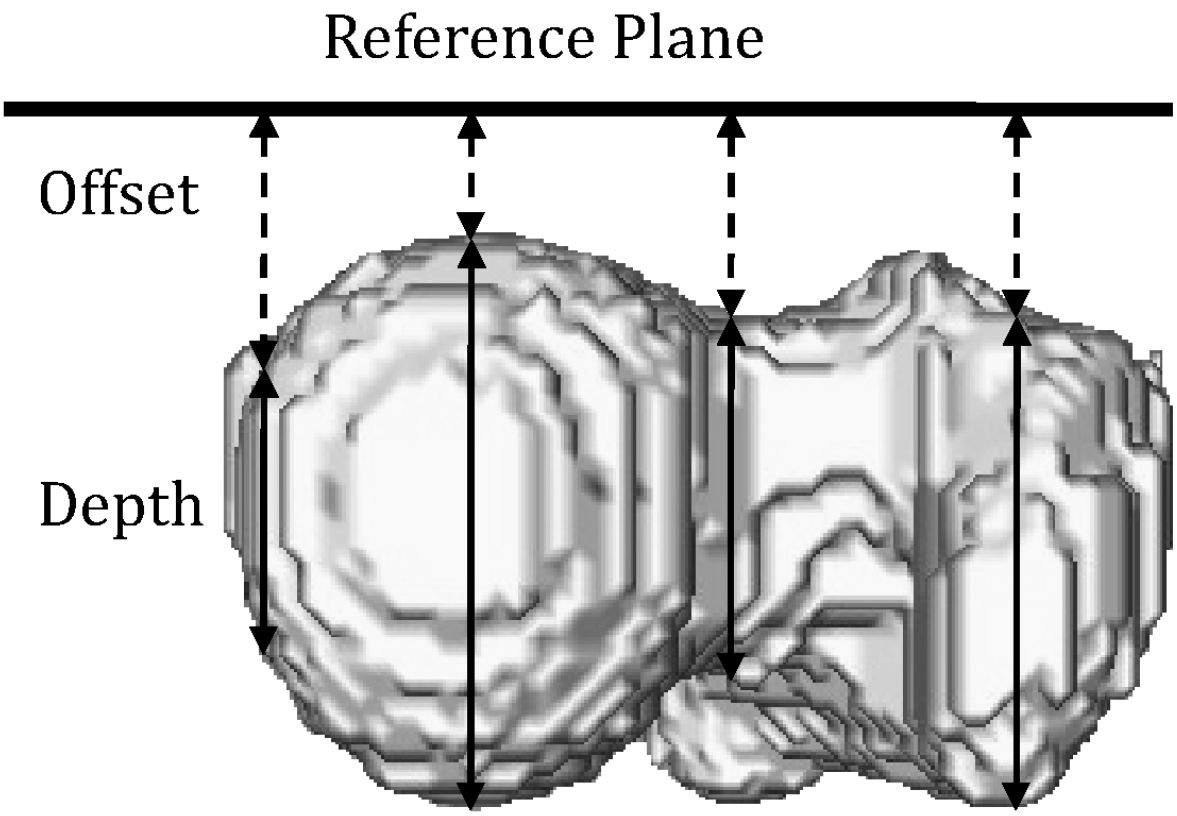


Figure 2: Description of Offset and Depth Maps

**Landmark Registration**

The first step in geometric morphometrics is the acquisition of landmarks for the shapes being analysed. Landmarks have been defined as “discrete homologous anatomical loci that do not alter their topological positions relative to other landmarks, provide adequate coverage of the morphology, can be found repeatedly and reliably, and lie within the same plane” **[20]**. Landmarks are typically chosen to quantify at least all the visible shape features required for analysis.

Figure 3 shows landmarks digitized along the outline of a 2D radiograph image of the human proximal femur. The landmarks in this case were chosen to provide an optimal number of visually recognizable points to describe the overall shape of the femur. Homology had to be ensured while selecting these landmarks for the various specimens and hence the landmarks

had to be clearly distinguishable along the image outline. Each radiographic projection in the input dataset was described by this ‘landmark configuration’.

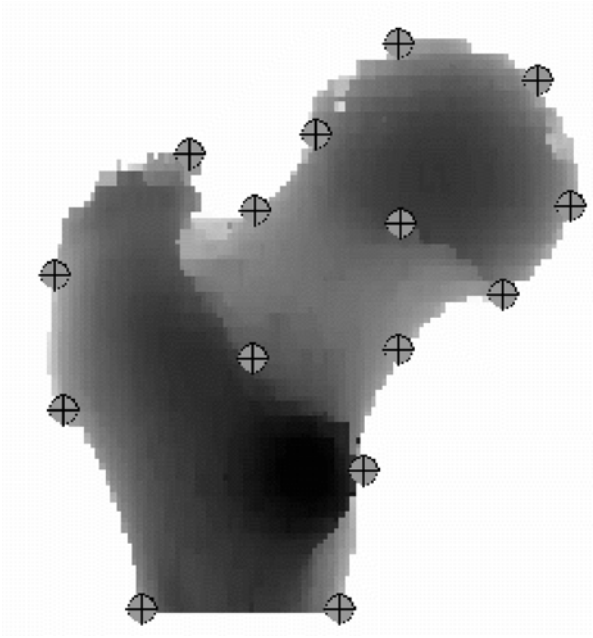

Figure 3: Landmarks on a 2D radiographic image of the proximal femur

**Creating the Shape Template using Generalized Procrustes Analysis and Thin Plate Splines**

Generalised Procrustes Analysis (GPA) **[21]** and Thin Plate Splines (TPS) **[22]** were employed to create the 3D shape template for the proximal femur. GPA was utilised to create an average 3D ‘Proximal Femur Training Template’ that could be expanded or contracted to suit the size and shape of an individual 2D ‘Test’ radiographic image. TPS deformation was applied to warp the 2D contour to match the radiographic projection of each input bone. This approach assumes that there is a proportional change in bone depth corresponding to a change in the overall bone size.

The average size and shape of the ‘Training’ 3D shape template was derived utilising Generalized Procrustes Analysis, that filtered out the Euclidean variations among the 2D projections of the samples. Each projection was described by a ‘landmark configuration’. The positional variation was removed by translating the centroid of each projection (calculated as

the mean of its co-ordinates) to the origin. Each of the projections was then scaled to its respective unit centroid size (calculated as the square root of the sum of the squared distances of the landmarks from the centroid) to filter out the scaling factor. They were iteratively rotated to the mean configuration computed at each pass to align their orientations. This procedure was applied to the offset and depth maps. Thin Plate Splines were then employed to visualize shape changes over the entire form instead of just the relative changes at landmark positions as obtained from the Generalised Procrustes Analysis. 3D grids describing the shape of the bone were built by merging the offset and depth maps. The TPS deformation was then carried out in two stages. In the first stage, they were used to compute the deformation from the landmark configuration for each individual bone to the mean configuration, the TPS therefore approximating the deformation between shapes using a smooth interpolating function of a linear combination of components that describe the patterns of relative landmark displacement. In the second stage, the resultant transformation matrix was applied to the offset and depth map for each femur, thus warping it to the mean shape. The resulting images were then averaged to create the average offset and depth maps from which the average 3D shape template was generated. This process of creating the average 3D shape template of the proximal femur from the Training cohort is shown in Figure 4.

The three CT datasets were randomly split into ‘Training’ and ‘Test’ cohorts. Two average 3D shape templates were created, one from 9 femurs within CT set (a), with 1.08-mm pixels and one from 13 femurs within CT sets (b) and (c), with 0.674-mm pixels.

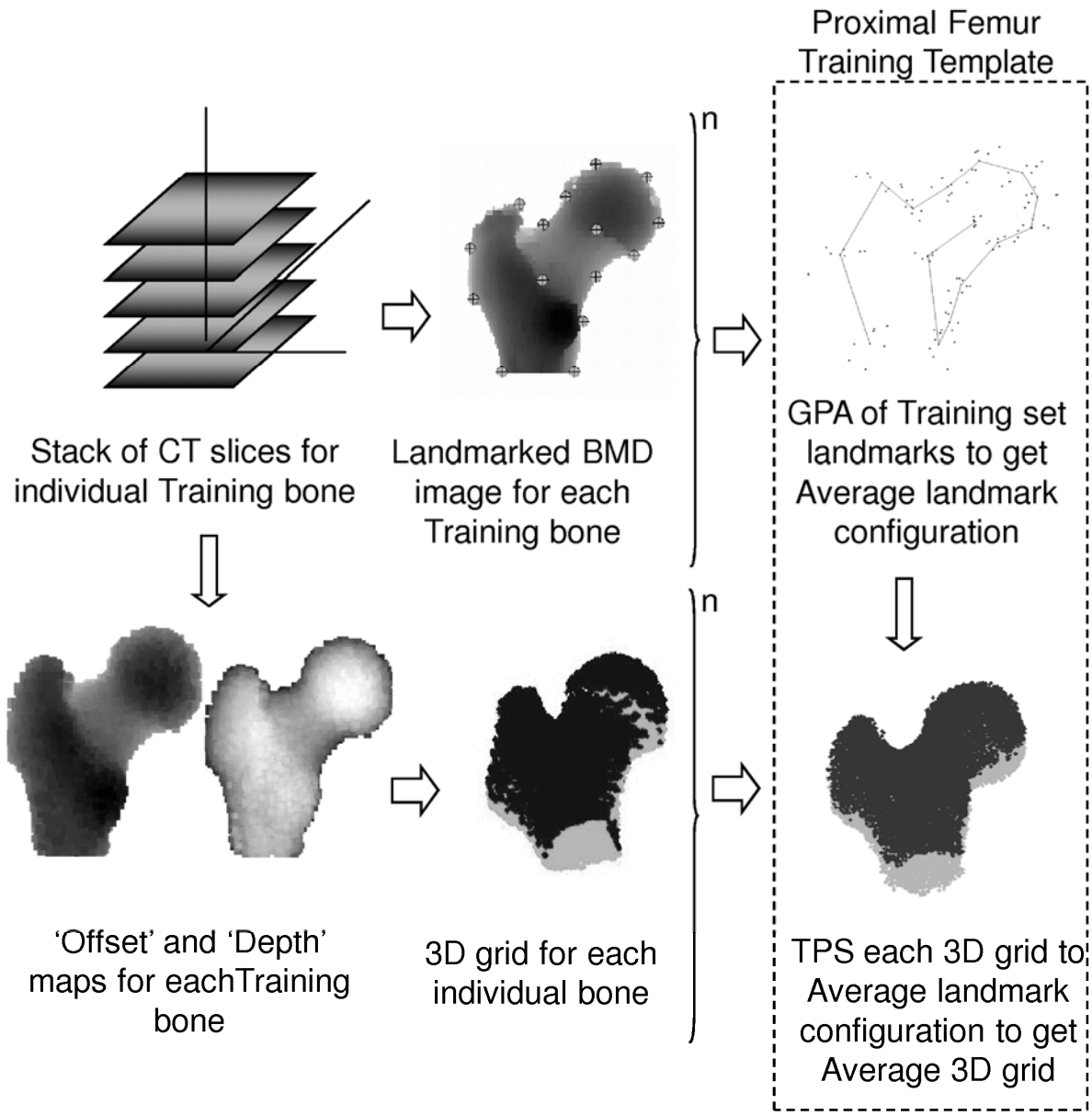


Figure 4: Overview of average 3D shape template creation. Two templates were created, one from 9 femurs within CT set (a), 1.08-mm pixels and one from 13 femurs within sets (b) and (c), 0.674-mm pixels.

**Applying the Shape Template to an Individual 'Test' Image**

The Test cohort consisted of the remaining 9 femoral CT scans from set (a) and 11 from sets (b) and (c), from which 2D projection images were derived and landmarked. For each Test femur, the landmark configuration of the average 3D shape template was first aligned to the landmark configuration of the Test 2D radiographic image using GPA. The average 3D

shape template was then warped using TPS, resulting in the creation of a 3D shape for each Test proximal femur. This process is illustrated in Figure 5.

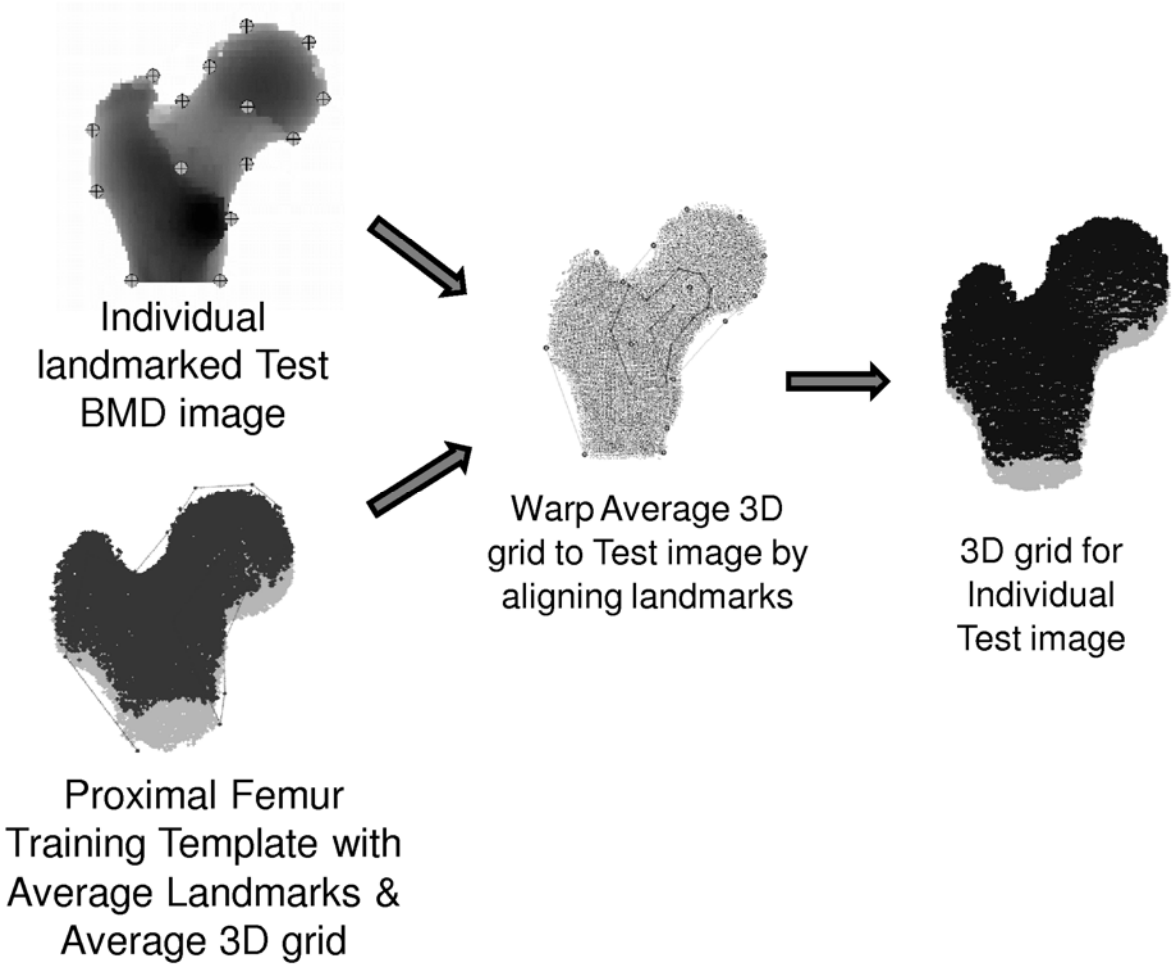


Figure 5: Transformation of the average 3D shape template to an Individual 2D radiographic Projection to create an individual 3D shape.

The measure of similarity between 2D landmark configurations was computed as an expression of the Euclidean distance, $d_{ik}$, [**23**] between the compared shapes i & k (in this case, the original and predicted shape respectively) computed as:

$$d_{ik}^2 = \sum (x_{ij} - x_{kj})^2 = s_{ii} + s_{kk} - 2s_{ik} \qquad \text{Equ. 1}$$

where j = 1 : p, p was the number of variables and $s_{ik}$ was the measure of the similarity between shapes i and k computed from the similarity matrix S = XX.

**Results**

Utilising the 2D similarity measure described above, the shape template technique had an accuracy of 99.75% to determine the Euclidean distance between corresponding landmarks. Thus, the created 2D shape profile was found to be a near-perfect match to the original 2D radiographic image for each individual proximal femur.

2D maps of absolute error for depth and offset, computed as the modulus of the per-vertex distance in 3D space between the predicted and original maps, are shown in Figure 6, with a comparison of original and generated 3D shapes shown in Figure 7. Hence, the depth and offset derived for each proximal femur from the shape template technique were compared with those correspondingly obtained from the original 3D CT data.

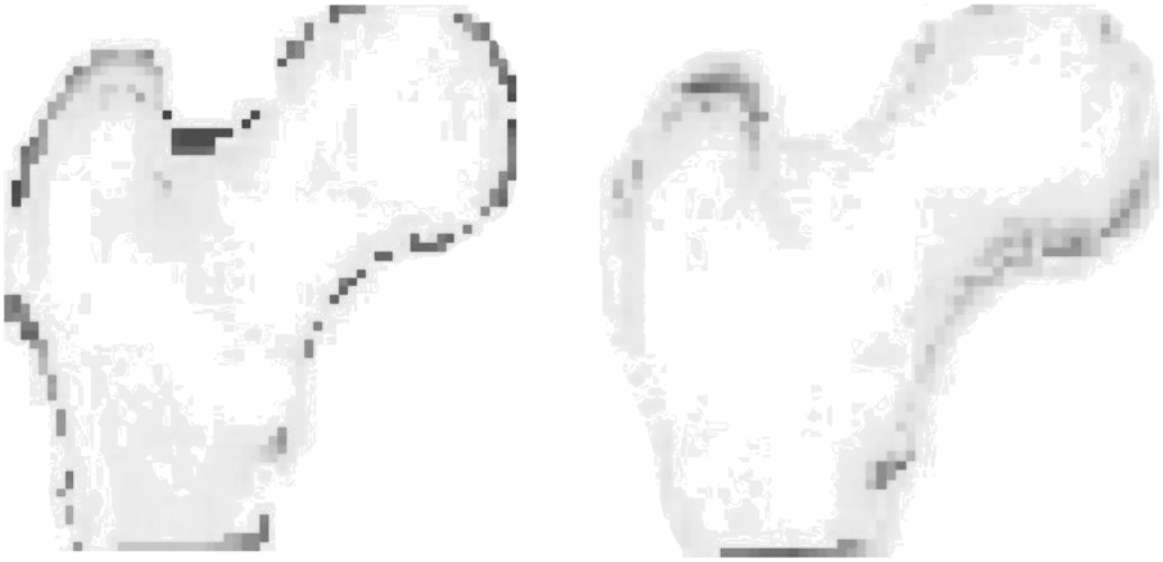

Figure 6: Offset and depth error maps. Pixels of darker shade of grey indicate higher absolute errors. The dimensional scale for the 256 grey levels within a single error map was described by separately reported minimum (0 grey) and maximum (255 grey) error values.

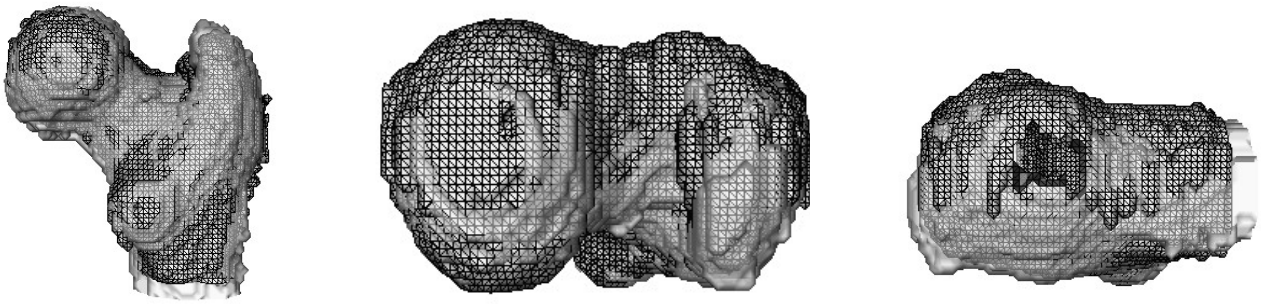

Figure 7: Visual representation in three orthogonal planes of the s
proximal femur (shown as light pixels) along with deviations observed within the proximal femur that was created from a single 'BMD' image utilising the Shape Template (shown as dark pixels).

The mean and standard deviation values for absolute depth and offset error (E) were derived using the following expression:

$$E = \frac{1}{p}\left|\begin{pmatrix} x_{i,predicted} \\ y_{i,predicted} \\ z_{i,predicted} \end{pmatrix} - \begin{pmatrix} x_{i,original} \\ y_{i,original} \\ z_{i,original} \end{pmatrix}\right| \qquad \text{Equ. 2}$$

where p describes the number of vertices considered.

The absolute depth and offset error data is summarised in Table 1.

Table 1: Mean and standard deviation values for depth and offset absolute errors within Test cohorts

| | CT Matrix Size | CT Pixel Size (mm) | Depth (mm) Mean ± SD | Depth Error (mm) Mean ± SD | Offset (mm) Mean ± SD | Offset Error (mm) Mean ± SD |
|---|---|---|---|---|---|---|
| n = 9 | 320 x 320 | 1.08 | 22.35 ± 1.74 | 3.40 ± 1.45 | 19.64 ± 1.47 | 2.97 ± 1.30 |
| n = 11 | 512 x 512 | 0.674 | 33.84 ± 6.37 | 1.73 ± 0.51 | 26.29 ± 3.30 | 1.33 ± 0.53 |

**Discussion**

This paper describes what is believed to be the first report of the generation of 3D proximal femur shapes from single projection 2D radiographic images.

The 2D projected contour of each generated shape was nearly identical to the contour of the respective original shape. The mean absolute depth errors of 3.4 mm and 1.73 mm for the 1.08 mm and 0.674 mm CT pixel sizes respectively are comparable to the mean absolute depth error of 0.8 mm reported by Kolta **[15]** using biplanar DXA reconstruction, noting that their pixel size was only 0.25 mm. Similarly, we utilised a CT slice thickness of 3 mm whereas Kolta et al utilised a 1.25 mm slice thickness. Hence, there is an inherent spatial resolution limitation of the original 3D CT that will have a direct influence on the accuracy of the shape template technique data. This is evidenced by the mean depth and offset errors being approximately a factor of two higher when the source CT data had a reduced spatial resolution by a factor of 1.6. Further, comparing the current 0.674 mm resolution CT data, Kolta reported a depth error factor of 2.2 for CT data with an improved spatial resolution by a factor of 2.7. Maximum depth and offset errors were observed (Figures 6 and 7) at the edges of the bone where there was minimum bone depth; again potentially dependent upon the spatial resolution of the source 3D CT data.

When generating a 3D shape from a 2D radiographic image using the technique described here, there is an assumption that the change in bone depth corresponds to a proportional change in the 2D parameters of bone length and width. We accept that this may not be so for all proximal femur shapes, particularly those at the ends of the shape spectrum, namely short stocky bones and long slender bones. However, for the majority of subjects, the hypothesis that bone depth could be predicted from its length and width proved reasonable.

A limitation of this study is that it was based upon a relatively small dataset of 23 proximal femurs for the training cohort and 20 proximal femurs for the test cohort, noting that each of these were further divided into two categories based upon CT pixel resolution. It is

considered reasonable to assume that a more representational and hence more accurate average 3D shape template would be derived if larger cohorts of training and test proximal femurs were considered in the future.

Both the training and test cohorts were derived from subjects of mixed sex but similar ethnic background, namely Caucasian. It is considered quite feasible that specific average 3D shape templates may have to be derived to accommodate age, sex and ethnic differences. Several studies have looked at variation of bone shape between ethnic and gender groups as well as with age. Ward et al. found that there were differences in bone geometry, BMC and volumetric BMD at the radial diaphysis between South Asian and European women of UK origin which were not explained by differences in body size [**23**]. Ethnic differences were also found to contribute to bone mass and fracture risk in a study of 197,848 community-dwelling postmenopausal women by Barrett-Connor et al [**25**]. African-American and Asian women were found to have 50% and 70% lower fracture risk respectively compared to Caucasian, Hispanic and Native American women. Meta et al. showed age-related differences in bone geometry among healthy women in two distinct age groups [**26**]. Bone mineral content and bone mineral density values were seen to differ significantly between the 28 young and 124 elderly healthy Caucasian women, with cross-sectional area and volumes at skeletal sites such as the trochanter and femoral neck found to be larger in the elderly than younger subjects Mayhew et al. [**27**] found substantial thinning of the cortical shell at the femoral neck area with aging, that declined less among men than women.

This study has demonstrated the potential for the application of a 3D shape template of the proximal femur to a single projection 2D radiographic image, such as that obtained by a DXA scan, in order to generate a 3D shape of the scanned proximal femur. It should be noted that the 2D radiographic images were derived from 3D QCT data and that unfortunately, DXA scan data for the excised femora was not available. DXA images may however be readily utilised within the described technique and future work could consider a clinical comparison using DXA and QCT images from patients.

Since the technique utilises a single 2D radiographic image such as a DXA scan, it is inherently sensitive to variability in anatomical positioning of the proximal femur. This sensitivity should be investigated in the future, ideally considering positional variation observed within the routine clinical environment.

Potential future applications of the 3D shape generation technique include derivation of volumetric density from areal bone mineral density and 3D finite element analysis for prediction of the mechanical integrity of the proximal femur. There is also the potential to apply this technique to other anatomical bone sites such as the distal radius and lumbar spine, again providing the potential to derive volumetric density from a single 2D DXA measure of areal bone mineral density.

**References**


1. Njeh CF, Fuerst T, Hans D, Blake GM, Genant HK (1999) Radiation exposure in bone mineral density assessment. Applied Radiation and Isotopes 50:215-36
2. Carter DR, Bouxsein ML, Marcus R (1992) New Approaches for Interpreting Projected Bone Densitometry Data. Journal Bone Mineral Research 7:137-45
3. Jergas M, Breitenseher M, Gluer CC, Yu W, Genant HK (1995) Estimates of Volumetric Bone Density from Projectional Measurements Improve the Discriminatory Capability of Dual X-ray Absorptiometry. Journal Bone Mineral Research 10:1101-10
4. Cvijetic S, Korsic M (2004) Apparent Bone Mineral Density estimated from DXA in Healthy Men and Women. Osteoporosis International 15: 295-300
5. Duboef F, Pommet R, Meunier PJ, Delmas PD (1994) Dual-Energy X-ray Absorptiometry of the Spine in Anteroposterior and Lateral Projections. Osteoporosis International 4:110-16
6. Sabin MA, Blake GM, MacLaughlin-Black SM, Fogelman I (1995) The Accuracy of Volumetric Bone Density Measurements in Dual X-ray Absorptiometry. Calcified Tissue International 56:210-14
7. Peel NFA, Eastell R (1994) Diagnostic Value of Estimated Volumetric Bone Mineral Density of the Lumbar Spine in Osteoporosis. Journal Bone Mineral Research 9:317-20
8. Boyanov M, Popivanov P, Gentchev G (2002) Assessment of Forearm Volumetric Bone Mineral Density from Standard Areal Densitometry Data. Journal Clinical Densitometry 5:391-402
9. Leslie WD, DeVos G, Dupont JO, Peterdy AE (2001) Reproducibility of Volume-Adjusted Bone Mineral Denity of Spine and Hip from Dual X-ray Absorptiometry. Journal Clinical Densitometry 4:307-12
10. Yan-Li Hou, Xian-Ping Wu, Xiang-Hang Luo, Hong Zhang, Xing-Zhi Cao, Y.-B. Jiang, Er-Yuan Liao (2007) Differences in age-related bone mass of proximal femur between Chinese women and different ethnic women in the United States. J Bone Miner Metab 25:243–52

11. Caponetti I, Fanelli AM (1990) 3D bone reconstruction from two x-ray views. In Proc. IEEE Conf. Eng. in Medicine and Biology, pp 208–10
12. Nikkhade-Dehkordi B, Bro-Nielsen M, Darvann T, Gramkow C, Egund N, Hermann K (1996) 3D reconstruction of the femoral bone using two x-ray images from orthogonal views. In Proc. Computer Assisted Radiology (CAR'96), pp 1015, Paris, France
13. Foley JD, Dam AV, Feiner SK, Hughes JF (1990). Computer Graphics: Principles and Practice, 2nd edition. Addison-Wesley,
14. Laporte S, Skalli W, D. G. J. A, F. Lavaste, and D. Mitton (2003) A biplanar reconstruction method based on 2D and 3D contours-application to the distal femur. Computer Methods in Biomechanics and Biomedical Engineering 6:1-6
15. Kolta S, Le Bras A, Mitton D, Bousson V, De Guise JA, Fechtenbaum J, Laredo JD, Roux C, Skalli W (2005) Three-dimensional X-ray absorptiometry (3D-XA): a method for reconstruction of human bones using a dual X-ray absorptiometry device. Osteoporosis International 16:969-76
16. Kendall D (1977) The diffusion of shape. Advances in Applied Probability 9:428–30
17. Zheng G, Ballester M, Styner M, Nolte L (2006). Reconstruction of patient-specific 3D bone surface from 2D calibrated fluoroscopic images and point distribution model. In Proc. International Conference on Medical Image Computing and Computer-Assisted Intervention, pp 25–32. Springer Berlin / Heidelberg
18. Lang P, Steiger P, Faulkner K, Gleuer C, Genant HK (1991) Osteoporosis: Current techniques and recent developments in quantitative bone densitometry. Radiol Clin North Am 29:49–76
19. Keyak JH, Kaneko TS, Tehranzadeh J, Skinner HB (2005) Predicting proximal femoral strength using structural engineering models. Clinical Orthopaedics & Related Research 437:219–28
20. Zelditch ML, Swiderski DL, Sheets HD, Fink WL (2004) Geometric Morphometrics for Biologists - A Primer. Elsevier Academic Press

21. Rohlf FJ (1990) Rotational fit (Procrustes) methods. In Rohlf FJ, Bookstein FL (eds) (1990) Proceedings of the Michigan Morphometrics Workshop, number 2, University of Michigan
22. Bookstein FL (1989) Principal warps-thin-plate splines and the decomposition of deformations. IEEE Transactions on Pattern Analysis and Machine Intelligence 11 :567–85
23. Manly BFJ (2000) Multivariate Statistical Methods, 2nd edition. Chapman & Hall / CRC
24. Ward KA, Roy DK, Pye SR, O'Neill TW, Berry JL, Swarbrick CM, Silman AJ, Adams JE (2007) Forearm bone geometry and mineral content in UK women of European and South-Asian origin. Bone 41:117–21
25. Barrett-Connor E, Siris ES, Wehren LE, Miller PD, Abbott TA, Berger ML, Santora AC, Sherwood LM (2005) Osteoporosis and fracture risk in women of different ethnic groups. Journal of Bone and Mineral Research 20:185–94
26. Meta M, Lua Y, Keyak JH, Lang T (2006) Young-elderly differences in bone density, geometry and strength indices depend on proximal femur sub-region: A cross sectional study in Caucasian-American women. Bone 36:152–58
27. Mayhew PM, Thomas CD, Clement JG, Loveridge N, Beck TJ, Bonfield W, Burgoyne CJ, Reeve J (2005) Relation between age, femoral neck cortical stability and hip fracture risk. Lancet 366:129-35